Functionalized Polyelectrolytes Assembling on Nano-BioFETs for Biosensing Applications

Xuexin Duan, Luye Mu, Sonya D. Sawtelle, Nitin K. Rajan, Ziyu Han, Yanyan Wang, Hemi Qu, and Mark A. Reed*

A new surface functionalization scheme for nano-Bio field effect transistors (FETs) using biocompatible polyelectrolyte thin films (PET) is developed. PET assemblies on Si nanowires (Si-NWs) are driven by electrostatic interactions between the positively charged polymer backbone and negatively charged Si/SiO_2 surface. Such assemblies can be directly coated from PET aqueous solutions and result in a uniform nanoscale thin film, which is more stable compared to the conventional amine silanization. Short oligo-ethylene glycol chains are grafted on the PETs to prevent nonspecific protein binding. Moreover, the reactive groups of the polymer chains can be further functionalized to other chemical groups in specific stoichiometry for biomolecules detection. Therefore, it opens a new strategy to precisely control the functional group densities on various biosensor surfaces at the molecular level. In addition, such assemblies of the polymers together with the bound analytes can be removed with the pH stimulation resulting in regeneration of a bare sensor surface without compromising the integrity and performance of the Si-NWs. Thus, it is believed that the developed PET coating and sensing systems on Si-NW FETs represent a versatile, promising approach for regenerative biosensors which can be applied to other biosensors and will benefit real device applications, enhancing sensor lifetime, reliability, and repeatability.

1. Introduction

Nano-BioFETs are field-effect transistor-based biosensors which have at least one dimension at nanoscale.[1] Due to their high surface to volume ratios and unique properties derived from spatial confinement, nano-BioFETs have shown great promise in electrical detection of (bio)molecular interactions. Nano-BioFETs have significant advantages over conventional optical methods due to their high sensitivity, minimum sample consumption, high throughput, and real-time detection without the need for labeling.[2] Nanotubes,[3] 1D semiconductor nanowires,[4] conductive polymer wires,[5] graphene,[6] and other 2D nanomaterials[7] have been used as the active channel in nano-BioFETs through bottom-up approaches.[8] Wafer scale nano-BioFETs have been successfully fabricated through complementary metal oxide semiconductor (CMOS) compatible top-down microfabrication process which facilitates the mass production of such devices.[9] In any case, nano-BioFETs share the same sensing principle by affinity-based detection, whereby the (bio)receptors are immobilized on the device surface. When analytes bind to these receptors, they produce variations in the surface potential, which can be detected as a shift in the threshold voltage or a change in the sub-threshold swing of the transistor characteristics.[10]

Surface functionalization of the nano-BioFETs with (bio) receptors plays a vital role in their biosensing performance.[11] The orientation, stability, accessibility, and functionality of the receptor molecules (antibodies, enzymes, DNA, etc.) greatly influence the overall performance of the sensor (the measurement reproducibility, sensor sensitivity, specificity, and reusability etc.).[12] Currently, silane chemistry (i.e., the reaction between hydroxyl terminated surfaces, such as SiO_2, and organosilanes) followed by the attachment of the (bio)receptors (i.e., via amine coupling) are largely applied to functionalize nano-BioFETs.[13] Despite the relatively easy modification process, disadvantages of silanization include: 1) silane tends to react with each other via cross-linking of the alkoxy units, resulting in rough, defective and unordered multilayers;[14] 2) silanization of metal oxide are very unstable in aqueous solutions due to the aqueous hydrolysis of the alkoxysilanes thus suffering degradation over time;[15] 3) proteins can nonspecifically adsorb to silanized surfaces, thus additional blocking steps are often needed post-functionalization to reduce background signals;[16] 4) covalent silanization is irreversible and functionalized devices can be (practically) used only once.[12] In addition, silane chemistry suffers from poor control of the loading efficiency, layer density, accessibility, stability, and orientation of the receptors.[17] These surface effects result in sensor baseline

Prof. X. Duan, Z. Han, Dr. Y. Wang, Dr. H. Qu
State Key Laboratory of Precision Measuring Technology and Instruments
College of Precision Instrument and Opto-Electronics Engineering
Tianjin University
Tianjin 300072, China
E-mail: xduan@tju.edu.cn
Prof. X. Duan, L. Mu, S. D. Sawtelle, Dr. N. K. Rajan, Prof. M. A. Reed
Department of Electrical Engineering
Yale University
New Haven, CT 06520, USA
Prof. M. A. Reed
Department of Applied Physics
Yale University
New Haven, CT 06520, USA

DOI: 10.1002/adfm.201500002

drift, false positives, irreproducible sensing, and other malfunctions of the nano-BioFETs.[18]

Apart from covalent functionalization, physical adsorption of polyelectrolytes (PETs) to the sensor surface has been demonstrated as an efficient approach for surface (bio)modifications.[19] Grafted copolymers PLL-*g*-PEG synthesized by grafting Poly-ethylene glycol (PEG) onto Poly-*L*-Lysine (PLL) backbones have been applied as the blocking layer to prevent protein nonspecific adsorption.[20] Since PLL is cationic at physiological pH, it can be electrostatically adsorbed to negatively charged surfaces, while the grafted hydrophilic PEG chains act as a barrier to prevent nonspecific protein adsorption. Though PLL-*g*-PEGs are only physically attached to the surface, their assembly is very stable due to the multivalent character of the interaction.[21] In addition, some of the PEG chains in PLL-*g*-PEG can be end functionalized with receptors.[22] This allows critical control over the biosensing interfaces by creating mixed monolayers with different functionalities.[23] In principle, PLL-*g*-PEG can be applied to nano-BioFETs, since most of the FET channels are covered with negatively charged metal oxides as dielectric. However, the rather long and large distributed PEG side chain (usually $\bar{M}_w$ > 2000 Da, length > 9 nm[24] is not an optimal choice for nano-BioFET applications. The long PEG chain put bioreceptors far away from the surface, thus increasing the risk of charge screening during FET detection. In addition, the distribution character inherent in PEG's $\bar{M}_w$ is not beneficial to acquire uniform molecular layer and repeatable biosensing.[25]

In this work, we propose that the structurally similar PLL-*g*-PEG copolymers comprised of shorter PEG grafts-oligo ethylene glycol (OEG) can be assembled on the nano-BioFETs as a (bio)functionalized nanothin film, while simultaneously preserving the advantages of PLL-*g*-PEG. Since OEGs are small and have no molecular weight distribution in comparison with PEGs, they allow grafting to PLL with higher yields and better uniformity, thus producing better defined and more uniform layers after assembly on the sensor surface.[26] Both solution synthesis and surface grafting were used to prepare PLL-*g*-OEG with different compositions of OEGs. Their surface stability and protein-blocking capacity were studied by electrical measurement with CMOS compatible Silicon Nanowire FETs (Si-NW FETs). To demonstrate the use of this class of copolymers in protein sensing, biotin was attached to the end of the OEG to form functional PLL-*g*-OEG-Biotin copolymers. Such graft copolymers were assembled on Si-NW FETs to detect streptavidin (SAv). Different graft ratios of biotin groups on PLL-*g*-OEG-Biotin have been synthesized and compared for their detection limits. In addition, surface regeneration of PLL-*g*-OEG-Biotin functionalized Si-NW FETs was tested by removal of assembled PETs through pH stimulations.

2. Results and Discussion

2.1. Synthesis and Characterizations of PLL-*g*-OEG and PLL-*g*-OEG-Biotin Copolymers

In this work, two sets of graft copolymers PLL-*g*-OEG and PLL-*g*-OEG-Biotin were prepared. The general architecture of polymers (**Figure 1**a,b) used in this work was based on a

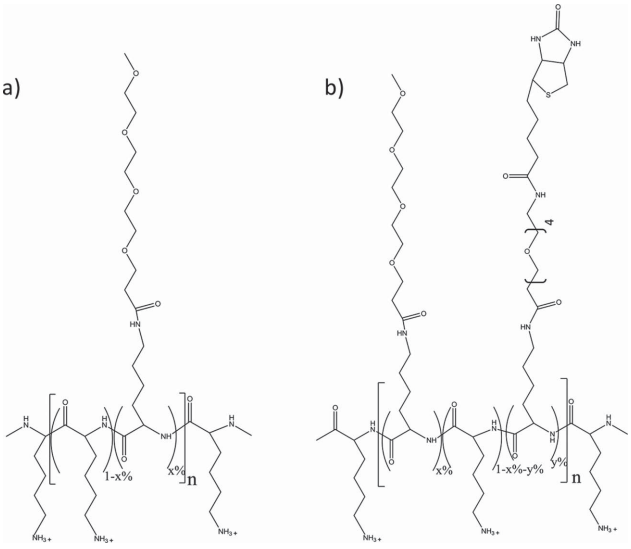

Figure 1. Chemical structure of a) PLL-*g*-OEG and b) PLL-*g*-OEG-Biotin.

PLL backbone of approximately 150 *L*-lysine units (average value in view of the poly dispersity of the polymer), and an OEG side chain of 4 ethylene glycol units with one end functionalized with either methoxy or biotin group. The polymers were prepared by reaction of NHS-OEG4 or NHS-OEG4-Biotin with PLL (15–30 kDa) (see also the Supporting Information). In slightly basic conditions (pH = 7–9), NHS reacts efficiently with primary amino groups ($-NH_2$) of the lysine residues by nucleophilic attack, forming an amide bond and releasing the NHS group. Five PLL-*g*-OEG copolymers with different OEG graft ratios (the ratio of OEG grafted PLL to the total PLL units, referred to as PLL-*g*-OEG-*x*%) were synthesized with OEG contents corresponding to *x* (%) = 10, 20, 30, 40, and 50 (**Table 1**). Eight PLL-g-OEG-Biotin copolymers with different OEG and OEG-Biotin graft ratios (referred to as PLL-g-OEG-*x*%-Biotin-*y*%) were synthesized with OEG contents corresponding to *x*(%) = 0, 5, 10, 15, 20, 25, 30, and 35, and OEG-Biotin contents represented by *y*(%) = 40, 35, 30, 25, 20, 15, 10, and 5. The total number of OEG side chains (whether biotin- or methoxy-terminated) is kept constant at 40% of all lysine residues, and the number of biotin-terminated OEG side chains is then a fraction of the total number of OEG chains. ^{1}H NMR was used to characterize the formation of such copolymers (see also the Supporting Information). The final grafting ratio (the percentage of the OEG or OEG-Biotin chains) was determined from the relative areas of the lysine side-chain peak ($-N-CH_2$) at 2.96 ppm and the OEG peak (CH_2-O-) at 3.65 ppm in ^{1}H NMR. Table 1 shows the real graft ratios of all the copolymers. It clearly proved the formation of such copolymers and the content of OEG or OEG-Biotin side chains were in agreement with the desired stoichiometric ratio. To allow us to easily refer to individual samples, we named the copolymers by their OEG or Biotin content (Polymer code, Table 1).

Under neutral pH condition, the PLL-*g*-OEG and PLL-*g*-OEG-Biotin are polycationic copolymers because of the nonreacted positively charged primary amine in the PLL backbone, and thus absorb spontaneously to negatively charged

Table 1. The copolymers used in this work and their selected physical properties after adsorption on Si/SiO_2 substrate (the water contact angle and film thickness data were averaged by three measurements using the same type of coating on different substrates).

Polymer type	Polymer name	Polymer code	OEG content [%]	Biotin content [%]	Thickness [nm]	Water contact angle [°]
PLL-*g*-OEG	PLL-*g*-OEG-10%	PLL-OEG_10	9.2	...	1.7 ± 0.7	45.2 ± 4.5
	PLL-*g*-OEG-20%	PLL-OEG_20	17.6	...	2.2 ± 0.5	48.4 ± 4.9
	PLL-*g*-OEG-30%	PLL-OEG_30	29.5	...	1.8 ± 0.4	42.7 ± 5.3
	PLL-*g*-OEG-40%	PLL-OEG_40	46.5	...	2.3 ± 0.8	37.3 ± 3.8
	PLL-*g*-OEG-50%	PLL-OEG_50	57.2	...	2.1 ± 0.7	38.6 ± 4.2
PLL-*g*-OEG-Biotin	PLL-*g*-OEG-35%-Biotin-5%	PLL-Biotin_5	41.8	3.2	1.8 ± 0.3	39.1 ± 5.1
	PLL-*g*-OEG-30%-Biotin-10%	PLL-Biotin_10	36.2	7.8	1.9 ± 0.3	41.8 ± 3.9
	PLL-*g*-OEG-25%-Biotin-15%	PLL-Biotin_15	29.3	16.2	2.5 ± 0.7	39.9 ± 4.8
	PLL-*g*-OEG-20%-Biotin-20%	PLL-Biotin_20	22.5	18.7	2.7 ± 0.9	44.2 ± 5.6
	PLL-*g*-OEG-15%-Biotin-25%	PLL-Biotin_25	26.3	22.7	1.7 ± 0.8	45.4 ± 4.3
	PLL-*g*-OEG-10%-Biotin-30%	PLL-Biotin_30	13.6	28.4	2.9 ± 0.3	34.6 ± 3.5
	PLL-*g*-OEG-5%-Biotin-35%	PLL-Biotin_35	4.2	33.8	2.1 ± 0.6	41.8 ± 5.3
	PLL-*g*-Biotin-40%	PLL-Biotin_40	...	46.4	1.9 ± 0.3	46.3 ± 5.6

substrate. In this work, water contact angle, ellipsometer, and AFM were used to characterize the copolymer thin films on flat silicon (Si/SiO_x) substrate. Table 1 shows the water contact angles of the copolymers coated flat silicon substrates. Both PLL-*g*-OEG and PLL-*g*-OEG-Biotin thin films showed hydrophilic properties. The corresponding contact angles of PLL-*g*-OEG decreased by increasing the OEG content and reached <40° after 40% PLL coupled with OEG. PLL-*g*-OEG-Biotin showed slightly higher contact angle due to the ended biotin group. However, there was no clear trend of the contact angle changes by increasing the biotin content. The thickness of the dry films was measured by ellipsometer (Table 1). This analysis resulted in an average thickness value of 2.02 ± 0.26 nm for PLL-*g*-OEGs and 2.18 ± 0.45 nm for PLL-*g*-OEG-Biotins which both indicated a monolayer formation on each substrate. AFM was applied to measure the film roughness of PLL-Biotin_40 coated silicon substrate (**Figure 2**). It clearly shows a uniform coating of PLL-Biotin_40 and the roughness is below 0.3 nm which is important in biosensing applications for BioFETs.

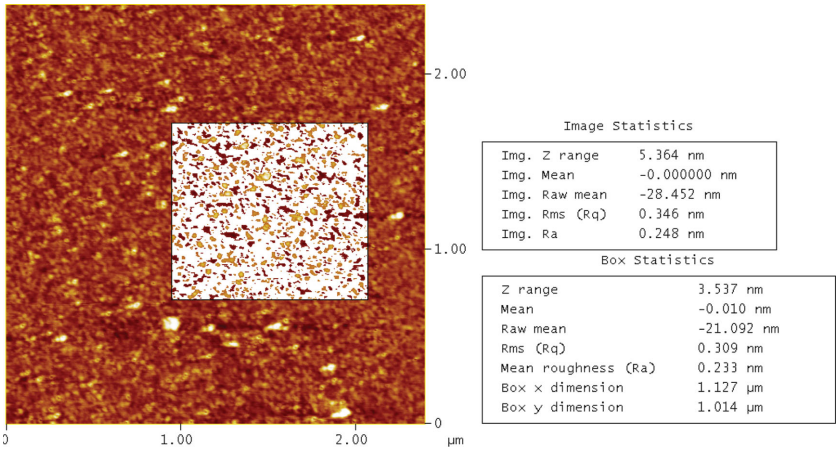

Figure 2. AFM image of PLL-Biotin_40 coated silicon substrate and surface roughness analysis.

2.2. Nonspecific Protein-Blocking Capacity of PLL-*g*-OEG Copolymers

The main concern regarding biosensor surface modifications is the protein nonspecific binding (NSB), which means that any protein present in solution will tend to bind to the biosensor's surface, thus leading to high background signals that cannot be differentiated from the intended specific binding.[27] Here, we first investigated the nonspecific protein blocking characteristics of PLL-*g*-OEG monolayers with different OEG side chain compositions using Si-NW FETs. Bovine serum albumin (BSA) was applied as a test protein since it is an abundant protein that is commonly used as a model protein and strongly adsorbs to non-modified substrates.[28] Si-NWFETs were coated with pure PLL or PLL-*g*-OEG with different OEG content (1 mg mL^{-1}), followed by incubation in BSA solutions (10×10^{-6} M, 0.01 × PBS, pH 7.4) for 15 min. The static *I*–*V* curve (*Id*_V_g scan) of the transistors was measured before and after BSA incubation. The threshold voltage shift of the devices was determined from the *I*–*V* curve and plotted against the compositions of the OEG side chains (**Figure 3**).

It clearly shows that the BSA adsorbs to the PLL coated Si-NWFETs resulting in a negative voltage shift (ΔV_T = –43.8 mV) of Si-NWFETs, which is due to the electrostatic interaction between negatively charged BSA and positively charged PLL. However, as soon as the device is modified with the PLL-*g*-OEG monolayer, the threshold voltage shift is reduced, indicating the amount of BSA that binds nonspecifically is decreased. After 40% PLL grafted with OEGs, the BSA nonspecific binding becomes insignificant (within the detection limit of Si-NWFETs). This confirms that the BSA is repelled by the PLL-g-OEG monolayers and the copolymer protein-blocking capacity increased with increasing OEG content. Additional fluorescent test of FITC labeled streptavidin (FITC-SAv,

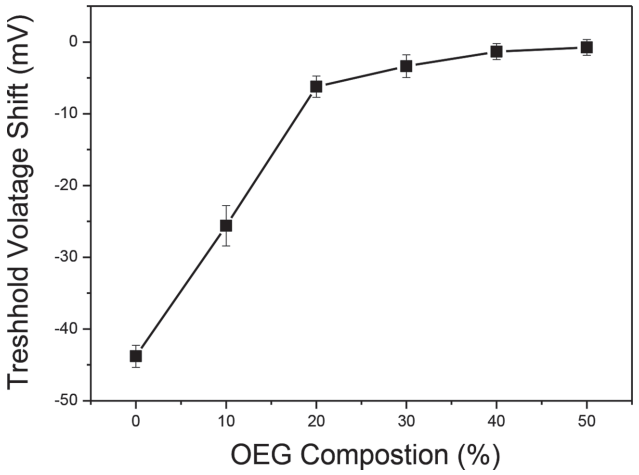

Figure 3. The sensor response of PLL-*g*-OEG coated Si-NW FETs to resist the BSA nonspecific binding.

0.1 mg mL^{-1}, 1 × PBS, pH 7.4) nonspecific adsorption on PLL-g-OEG*x* coated silicon substrate were measured by fluorescent microscopy which shows similar blocking capacity of PLL-g-OEG copolymers (see the Supporting Information, Figure S3). Such blocking capacity is likely due to the oligo (ethylene glycol) coating which is closely mimicking an aqueous solution, thus minimizing the possibility of hydrophobic effect. In principle, more OEG grafting for PLL-g-OEG copolymers is preferred in order to minimize nonspecific adsorption. However, covalent grafting of OEG groups consumes the quaternary amine groups from the lysine residues on the PLL, reducing the positive charge on the molecule. Since their positive charge plays a key role in their immobilization on negatively charged substrates, PLL-g-OEG layers tend to lose their adhesive properties with increased grafting of OEG. Therefore, we optimized the OEG graft ratio as 40% for PLL-g-OEGs in the rest of the work to balance their ability to prevent protein nonspecific adsorption and their ability to bind to the substrate.

2.3. Streptavidin Sensing

To demonstrate specific protein sensing using the OEG grafted copolymer, biotinylated PLL-*g*-OEG (PLL-*g*-OEG-Biotin) were used to functionalize the sensor and detect the target of Streptavidin (SAv). PLL-*g*-OEG-Biotin adsorb to surfaces through columbic interactions between positively charged PLL backbone and negatively charged Si/SiO_2, causing OEG chains terminated with biotin to extend into solution and act as specific reorganization sites for SAv binding . A series of copolymers of PLL-*g*-OEG-Biotin were prepared by a one-step solution phase reaction between NHS-OEG biotin and PLL at the desired stoichiometric ratio, followed by adsorption of the PLL-*g*-OEG-Biotin onto the sensor surface (Table 1). The intended control over the composition of PLL-*g*-OEG-Biotin presents a straightforward method at molecular-level to manipulate the biotin surface density and surface properties of the sensor surface which is rather important for surface based biodetection.

Here we first examined Si-NW FETs coated with a series of PLL-*g*-OEG-Biotin with different biotin compositions in terms of biotin surface density effects on SAv detection. As comparisons for Si-NWFETs, the patterned silicon substrates coated with the same copolymers were incubated in fluorescent-labeled SAv solution FITC-SAv and then investigated by fluorescent microscope. **Figure 4**a shows the real time electrical measurement of SAv by different biotin compositions of PLL-*g*-OEG-Biotin coated Si-NWFETs. After the biotinylation, 10×10^{-9} M of SAv (1×10^{-3} M HEPES) was introduced. The initial flat part in Figure 4a after adding the SAv indicates the flow reached the sensor. Then, the current increased quickly after contacted with SAvs which indicates the adsorption of SAv due to their negatively charged at pH 7.4 (PI ≈ 5.6). Figure 4b shows the fluorescent microscope images of the same copolymer coated silicon substrate after incubation with FITC-SAv (0.1 mg mL^{-1}). Exposure time is kept constantly at 500 ms. Fluorescent intensity of PLL-biotin-SAv (FITC) along the gold-silicon patterns of each image is analyzed by Image-Pro Plus and plotted in Figure 4c. Figure 4d plots the calibrated responses from Si-NW FETs (current changes divided by the device transconductance ($\Delta I/g_m$)) and the fluorescent intensity, using these two methods to confirm the amount of the absorbed SAv versus the percent biotinylation of the lysine residues of the functionalized PLL-*g*-OEG-Biotin.

As seen from Figure 4d, the SAv surface coverage increased with higher biotin surface density, and there is no further increase after 30% of biotinylation of lysine residues (PLL-Biotin_30), indicating a complete SAv monolayers (saturation) coverage is reached. It is also noticed that the SAv coverage is not a linear function of the biotin composition. If all of the biotin moieties in the PLL-*g*-OEG-Biotin monolayer were available for binding with SAv, the SAv coverage should increase linearly with the biotin surface density as seen in the case of PLL-PEG-Biotin. SAv is a homotetrameric protein with four identical biotin-binding sites, thus, steric effects have to be considered. Once the PLL-Biotin surface is covered with a significant amount of SAv, SAv molecules from solution have a difficult time finding an adsorption site that is not partially blocked. Nonetheless, at higher biotin density (graft ratio > 20%), a large excess of specific adsorption sites is provided, the steric hindrance problem is overcome, and a complete monolayer of SAv is formed at biotin graft ratio around 30%. This result also agrees with the previous studies using surface plasmon resonance (SPR) coated with mixed biotin-containing alkylthiolate monolayers which indicates a complete SAv layer forms at 34% of biotin coverage.[29] Control experiments were performed to verify that the SAv was specifically adsorbed onto the biotin sites present on the SiO_2 surface. No current change was observed when the PLL-*g*-OEG-Biotin surface was exposed to a solution of SAv that had been conjugated with D-biotin. Here PLL-*g*-OEG-Biotin also functions as a barrier to prevent the nonspecific adsorption of conjugated SAv.

We studied PETs coating of Si-NW FETs from two different approaches. One approach is referred as solution synthesis as mentioned above and the other is surface grafting. In the surface grafting, we attached PLL to the NW surface at first and then introduced NHS-OEG-biotin for grafting to the just attached PLL. The former approach is advantageous in the

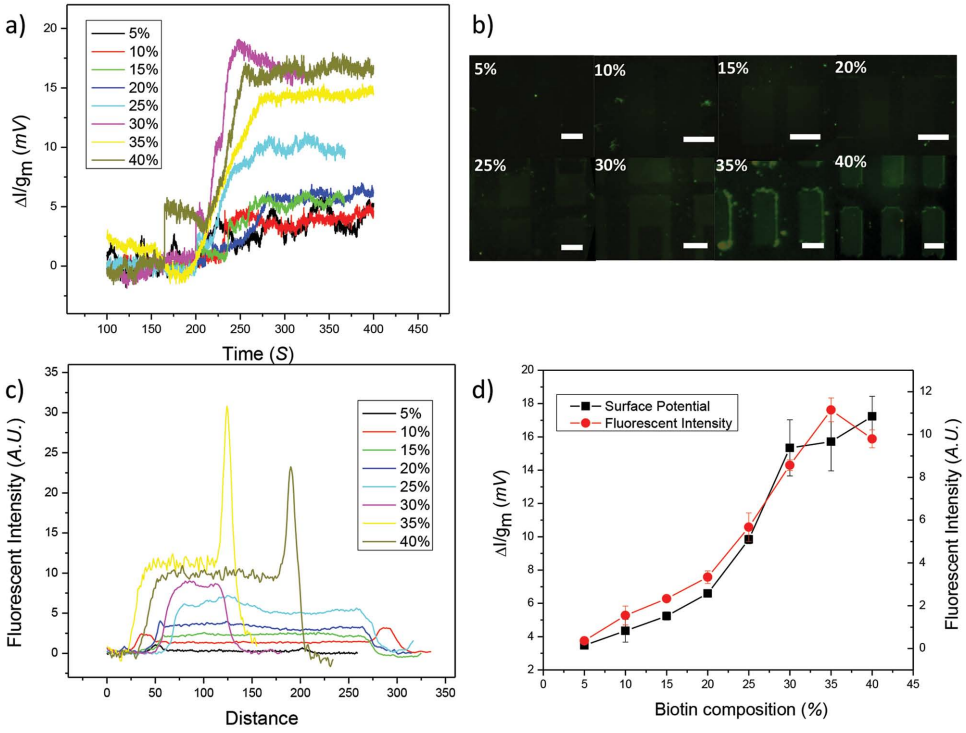

Figure 4. a) Sensor response of SAv sensing by Si-NW FETs coated with different biotin compositions of PLL-*g*-OEG-Biotin; b) fluorescent images; c) corresponding intensities along the gold–silicon patterns of different biotin compositions of PLL-*g*-OEG-Biotin coated silicon substrates for FITC-SAv detection; d) normalized responses from Si-NW FETs and the fluorescent intensity versus the percent biotinylation of the lysine residues of the functionalized PLL-*g*-OEG-Biotin. (The scale bar in (b) is 3 μm. The error bar of FET response is obtained by the average of the whole data points except the transition. The fluorescent intensity error bar is obtained by the average of each pattern except of the edge part.)

consideration of reproducibility, since it could provide precise control over the amount of biotin on the sensor surface and consequent SAv coverage (Figure 4d). In comparison, the latter, surface grafting, offer little control over biotinylation percentage of the PLL on the sensor surface (data not shown).

The SAv sensing with different compositions of biotin by PLL-g-OEG-Biotin coatings indicates a success in single molecular-layer control over the surface properties of the Si-NW FETs. Significantly, this work provides novel strategy to engineer sensor surface functional group densities and can be applied to all surface based sensors.

To further demonstrate the detection limit of PLL-*g*-OEG-Biotin coated Si-NW FETs, we functionalized the device with PLL-Biotin_35, followed by the detection of serially diluted SAv. **Figure 5** shows the real time sensor responses of SAv adsorption on PLL-Biotin_35 coated Si-NW FETs. The binding kinetics shows a consistent increase in the rate of association with higher concentration of streptavidin. Above picomolar range, the normalized sensor responses ($\Delta I/g_m$) at their equilibrium state reaches the same value (≈19 mV), suggesting the similar surface coverage of bound SAv is reached and the sensor is saturated at those concentrations. The sensor response at 500×10^{-15} M did not saturate within our measurement time (2 h), thus the binding is still in the linear regime of the exponential apparent. Nevertheless, the detection limit of the PLL-*g*-OEG-Biotin coated Si-NW FETs are comparable with the conventional silane monolayer coated devices.[30]

2.4. Sensor Regeneration

For charge sensing with nano-BioFETs, the reusability of the sensor often poses an issue, as high quality devices incur significant fabrication cost, and therefore cannot serve as one-time use sensors. Besides, due to the nanofabrication limits, variations in device characteristics from one sensor to another require calibrations for every device separately before their deployment in a real sensing application which largely hinder the practical applications of nano-BioFETs.[31] Strategies to overcome the issue involve developing specific chemistries to regenerate the BioFETs which means removing the absorbed analyte from the sensor surface with an active method after each measurement without sacrificing device performance. Supramolecular approach through cyclodextrin chemistry has been applied to regenerate the Si-NW FETs surface. However, such strategy requires multistep chemical synthesis and the orthogonal linker is difficult to fully remove from the sensor surface due to the multivalent interactions.[12]

Compared with the supramolecular approach, surface regeneration of physical absorbed PETs is rather straightforward. PLL-*g*-OEG adsorption relied on the columbic interaction between the positively charged PLL backbones and negatively charged Si/SiO_2 substrate. By changing the solution pH below the point of zero charge of Si/SiO_2 surface (PZC of Si/SiO_2 is around pH = 3), the surface is no longer negatively charged thus repelling the positively charged PLL and releasing the copolymers from the surface. In this work, we demonstrated the

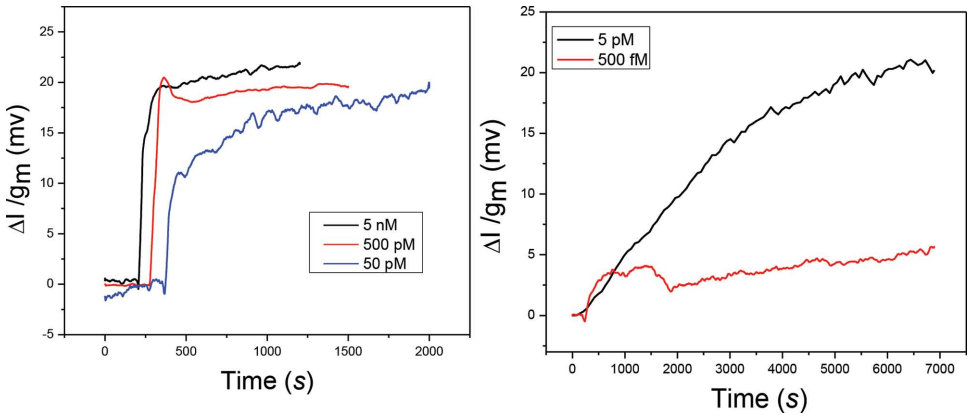

Figure 5. Real-time sensor responses of biotin–streptavidin binding with PLL-Biotin_35 coated Si-NW FETs.

surface regeneration of PLL-*g*-OEG-Biotin coated Si/SiO_2 substrate through pH controlled nanoparticle desorption and SAv sensing with Si-NW FETs. **Figure 6**a shows the SEM images of PLL-OEG_10 coated silicon nanowire after incubation in a solution containing 20 nm SiO_2 nanoparticles (NPs). Negatively charged SiO_2 NPs were uniformly adsorbed on the PLL-OEG coated device due to electrostatic interactions. After treatment with acidic buffer (pH = 2), the silica NPs are removed from the surface as shown in Figure 6b, suggesting the removal of PLL-OEG coating together with the adsorbed NPs.

As a direct proof for sensor regeneration, PLL-Biotin_35 coated Si-NW FETs were used to reversibly detect SAv. SAv removal from the sensor surface is very difficult, as SAv-biotin bond is considered as one of the strongest noncovalent interactions. Here, we demonstrated the detection of biotin-SAv using PLL-*g*-OEG-Biotin coated Si-NW FETs and subsequent removal of the entire SAv-bound PLL-*g*-OEG-Biotin coating with pH stimulations. Figure 6c shows the real time measurement of SAv detection on PLL-Biotin_35 coated Si-NW FET and surface regeneration with acidic buffer (pH = 2). After first incubation of SAv (10×10^{-15} M), the sensor was treated with buffer (pH = 2) for half hour. After pH of the solution was switched back to neutral (pH = 7), the sensor base line came to the same level as before PLL-Biotin_35 coating (dashed line in Figure 6c) thus proved the removal of the PLL-Biotin_35 layer together with the adsorbed SAv and the successful regeneration of the device. The device was further coated with PLL-Biotin_35 again and followed by second SAv detection. The sensor response is rather repeatable which indicates that the sensor characteristics are not influenced by our surface regeneration strategy. The demonstrated reversible binding of SAv on PLL-g-OEG-Biotin functionalized Si-NW FETs will allow the reuse of the sensors for multiple detections and such approach can work with any binding affinity system. Furthermore, the adsorbed SAv through PLL-g-OEG-Biotin enables the free biotins to be directed toward

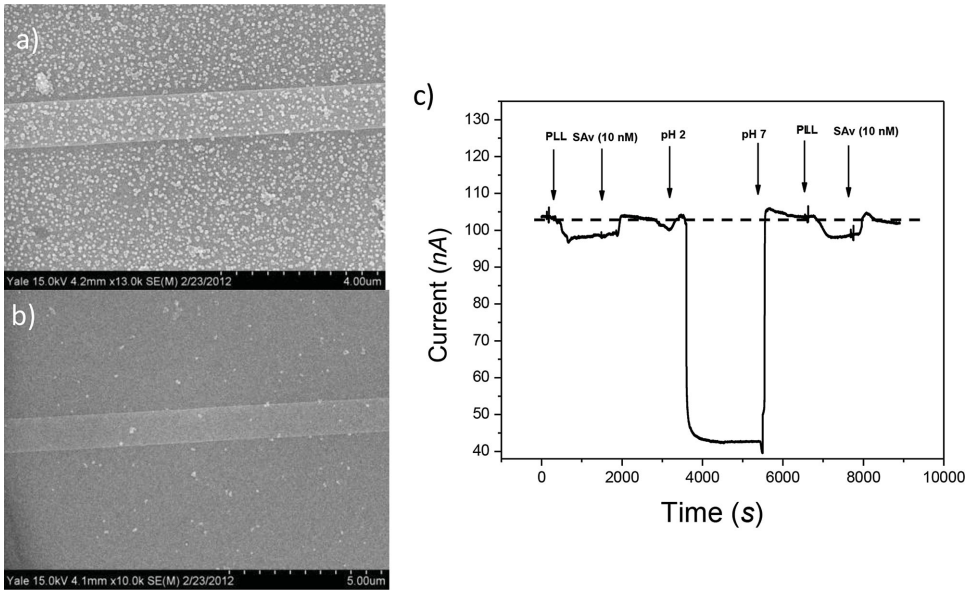

Figure 6. a) SEM images of silicon nanoparticles adsorbed on PLL-*g*-OEG coated Si-NWs, and b) after treatment of pH 2 buffer; c) real-time sensor responses of biotin–streptavidin binding and surface regeneration of PLL-Biotin_35 coated Si-NW FETs.

the solution, which could be used for binding of a variety of (bio)molecules through biotin-SAv chemistry to enable multiplexed protein detection.

Besides the reusability, the film stability of PLL based coating is another advantage. Conventional surface functionalization of the nano-BioFETs with (bio)receptors is silanizations either in solution or by vapor phase. Aminosilane-derived layers are observed to hydrolysis upon extensively exposed in water.[32] Such degradation will induce the sensor current drifting. To test the amino coating stability, we measured the surface nitrogen contents of aminosilane and PLL coated silicon substrate upon socking in water using ATR-FTIR (Supporting Information, Figure S5). It clearly shows that the fresh attached aminosilanes molecules are degraded completely upon socking in water for 48 h while the PLL coated substrate is rather stable under the same conditions. The rather stable PLL coating will allow the long-term storage of the functionalized sensors. We have used the same PLL-Biotin modified chip for more than 3 months without observing degradations of the chemical surface, whereas unprotected aminosilane coated chips typically only last 1 week.

3. Conclusion

In conclusion, we have demonstrated a new biosensing interface based on polyelectrolytes coating for nano-bioFETs. A series of PLL-*g*-OEG and PLL-*g*-OEG-Biotin with different compositions of short oligo-ethylene glycol and biotins have been successfully synthesized and the structures were verified by NMR. Assembly of such copolymers on negatively charged Si substrate formed uniform monolayers, and the thin films have been fully characterized by ellipsometer, water contact angle, optical microscopy, and AFM. Compared with conventional surface modification of nano-bioFETS by silane-based chemistry, the PET physical adsorption coating has the advantages of direct solution coating from polymer aqueous solutions which is simple and reliable and can be applied on a wafer scale. The ability of the PLL-*g*-OEG surfaces to prevent protein nonspecific binding was tested against nonspecific adsorption of BSA and the OEG composition has been optimized between nonspecific protein blocking capacity and surface stability of the coating. Si-NW FETs were functionalized with biotinylated PLL-*g*-OEG copolymers (PLL-*g*-OEG-Biotin), which were used to detect the protein streptavidin. The demonstrated sensing of SAv with different compositions of biotin group from PLL-*g*-OEG-Biotin coated devices represents a versatile, promising approach to precisely control the sensor surface functional group densities at the molecular level. Furthermore, the reversible sensing of SAv with pH controlled device regeneration represents a simple approach for surface regeneration without sacrificing device performance, which is very attractive both from a device performance and economical point of view, since it permits accurate calibration prior to measurements, and repeated use of the same calibrated device. More important, the developed PLL-*g*-OEG based PET surface coating can be largely applied to other surface based biosensors.

4. Experimental Section

Materials: All chemicals were of analytical grade and used as received without further purification. Phosphate buffered saline tablets (PBS, pH 7.4), 4-(2-hydroxyethyl)-1-piperazineethanesulfonic acid (HEPES), PLL (15–30 kDa), streptavidin labelled with fluorescein isothiocyanate (Streptavidin-FITC), and Bovine serum albumin (BSA) were purchased from Sigma-Aldrich. EZ-Link *N*-hydroxysuccinimidyl ester (NHS)-OEG4-Biotin and EZ-Link NHS-OEG4 were purchased from Thermo SCIENTIFIC. Streptavidin was purchased from ROCKLAND IMMUNOCHEMICAL. The lyophilized Streptavidin was restored with deionized water and diluted to the desired concentrations with buffers before using.

Synthesis of PLL-g-OEG and PLL-g-OEG-Biotin Copolymers: Synthesis of nonfunctionalized PLL-*g*-OEG graft copolymers was accomplished by reaction of NHS-OEG4 with PLL (15–30 kDa) (see also the Supporting Information). First, PLL was dissolved in 50×10^{-3} M sodium carbonate buffer (pH 8.5) at a concentration of 40 mg mL^{-1}. The solution was filtered through a 220 nm pore syringe filter. Solid n-hydroxysuccinimidyl ester of OEG4 was added to the dissolved PLL solution in the desired stoichiometric ratio under vigorous stirring. The reaction was allowed to proceed for 5 h at room temperature, after which the reaction mixture was dialyzed (molecular weight cut off 8 kDa; Spectrum, Rancho Dominguez, CA) against PBS at pH 7.4 for 24 h and subsequently against deionized water for 24 h. The dialyzed solution was lyophilized for 24 h and stored in freezer. The chemical structure of PLL-*g*-OEG was verified by (NMR). (^{1}H NMR in D_2O (see also the Supporting Information). δ [ppm] = 1.32–1.38 ((lysine γ-CH_2), 1.43–1.85 (lysine β, δ-CH_2), 2.50 (coupled OEG, –CH_2–C(O)–NH), 2.96 (free lysine, –N–CH_2), 3.17 (OEG activated lysine, C(O)–NH–CH_2–), 3.36 (OEG, –O–CH_3), 3.65 (OEG, CH_2–O–), 4.28 (lysine, NH–CH–C(O)–)). Biotin-functionalized PLL-*g*-OEG-Biotin copolymers were synthesized using the same method by reaction of NHS-OEG4-Biotin and NHS-OEG4 with the same PLL (15–30 kDa) in the desired stoichiometric ratio (^{1}H NMR in D_2O (see also the Supporting Information). δ [ppm] = 1.37–1.43 (lysine γ-CH_2), (biotin, β-CH_2–), 1.48–1.90 (lysine β,δ-CH_2), (biotin, γ-CH_2), 2.23 (biotin, –CH_2C(O)NH–), 2.40 (coupled OEG, –CH_2–C(O)–N), 2.66 (lysine,(–CH_2–C(O)–N)), 2.85–2.89 (lysine, –CH_2–NH–C(O)), (OEG, –CH_2–NH–C(O)), 3.06 (biotin, –S–CH_2–), 3.20 (biotin, –S–CH–), 3.27 (free lysine, –N–CH_2), 3.56 (OEG, CH_2–O–), 4.17 (lysine, N–CH–C(O)–), 4.30 and 4.48 (biotin, 2 bridge head CH)).

Si Nanowire FET Biosensor Fabrications: The devices were fabricated from 4 in. silicon on insulator (SOI) wafers (Soitec). The silicon active layer (p-type doping = 10^{15} cm^{-3}) was first thinned to about 45 nm by thermal oxidation and the silicon oxide was removed using wet etching (buffered oxide etch (BOE)). The source and drain regions as well as the back-gate were patterned by contact lithography and doped by BF^{2+} implantation. Following dopant activation in a furnace at 900 °C, the NWs were defined by optical lithography. The pattern was transferred to the active silicon layer using Cl_2 inductively coupled plasma etch (Oxford 100), or a CF_4 reactive-ion etch (Oxford 80). Top-gate oxidation is then performed using thermal oxidation to generate 20–30 nm silicon oxide on top of the nanowire. The devices were then metallized by aluminum evaporation and patterned by lift off. The metal contacts were annealed in a rapid thermal processor at 450 °C for 1 min and devices were measured to ensure the ohmic contacts. The final step was to passivate the devices with a 1 μm layer of SU8 photoresist with lithographically patterned openings at top of the devices, contact pads, and the solution gate electrode. The wafer was then hard-baked at 130 °C for 20 min.

Device Surface Functionalization: The Si-NW oxide surfaces were cleaned with UV ozone (UV/Ozone ProCleanerTM Plus, Bioforce Nanosciences) for 10 min before functionalization. PLL-*g*-OEG or PLL-*g*-OEG_4-Biotin copolymers were dissolved in 5×10^{-3} M HEPES solution (1 mg mL^{-1}, pH 7.4). The devices were incubated in the copolymer solutions for 20 min followed by rinsing with copious amounts of millipore water and dried in a stream of nitrogen. The amino silanization is coated by vapor phase deposition of (3-Aminopropyl) triethoxysilane (APTES) under reduced pressure in a desiccator.

Surface Characterizations: PLL copolymer coated flat silicon substrate was characterized by Fourier transform infrared (FTIR) spectrometer (Vertex 70v, Bruker Optics, Germany); water contact angle measurement (JC2000DM, Zhongchen), and ellipsometer (EMPro, ElliTop Scientific Co. LTD). To facilitate the fluorescence observation, micro gold–silicon patterns were fabricated to evaluation of the chemical functionalization by fluorescence microscopy (Olympus BX53). The morphology of the deposited thin films on silicon surface was characterized by Atom Force Microscopy (AFM) (Veeco, Nano Scope III) in tapping mode.

General Sensing Setup: The functionalized dies were packaged using 28-pin ceramic headers (Spectrum Semiconductor Materials). A fluid delivery system was then mounted on top of the dies and ensured fluid containment over the devices and isolation from the chip perimeter and bonding region. The mixing cells (solution chamber) were created by epoxying thin-walled, ≈5 mm diameter polytetrafluoroethylene (PTFE) tubing to the chip surface and by inserting thinner tubing (0.5 mm) to serve as the fluid supply and return. The solution input tube was placed directly over the central region of the die. This system enabled continual mixing (equivalent to pippetting up-and-down) throughout the course of sensing measurements. A miniature Reference Electrodes (Harvard Apparatus) was integrated as well. Multiplexed *I*–*V* and DC time measurements were carried out by a custom made system using a National Instruments Data Acquisition Card and Keithley 2636 Dual Source Measure Unit. For all measurements, I_{ds} was measured at 0.5 s intervals, while V_{ds} and V_g were held constant; V_{ds} was set to 0.1 V and V_g was set to ensure operation in the linear regime determined from I_d–V_g measurement before sensing.

Supporting Information

Supporting Information is available from the Wiley Online Library or from the author.

Acknowledgements

X.D. acknowledges the support by the "Tianjin AppliedBasic Research and Advanced Technology (14JCYBJC41500) and the 111 Project (B07014). M.A.R. acknowledges support by the (FA8650-9-D-5037 0019) and the Army Research Office (MURI W911NF-11-1-0024). L.M. acknowledges scholarship support from Natural Sciences and Engineering Council of Canada (NSERC). We are grateful to our colleagues Monika Weber and Weihua Guan for help with the electrical measurement and helpful discussions.

Received: January 1, 2015
Revised: February 6, 2015
Published online: March 4, 2015

[1] M. J. Schoning, A. Poghossian, *Analyst* **2002**, *127*, 1137.
[2] a) N. Elfstroem, A. E. Karlstroem, J. Linnrost, *Nano Lett.* **2008**, *8*, 945; b) E. Stern, A. Vacic, M. A. Reed, *IEEE Trans. Electron. Devices* **2008**, *55*, 3119.
[3] C. Han, A. Doepke, W. Cho, V. Likodimos, A. A. de la Cruz, T. Back, W. R. Heineman, H. B. Halsall, V. N. Shanov, M. J. Schulz, P. Falaras, D. D. Dionysiou, *Adv. Funct. Mater.* **2013**, *23*, 1807.
[4] Y. Cui, Q. Wei, H. Park, C. M. Lieber, *Science* **2001**, *293*, 1289.
[5] X. Duan, Y. Zhao, E. Berenschot, N. R. Tas, D. N. Reinhoudt, J. Huskens, *Adv. Funct. Mater.* **2011**, *20*, 2519.
[6] R. Stine, S. P. Mulvaney, J. T. Robinson, C. R. Tamanaha, P. E. Sheehan, *Anal. Chem.* **2013**, *85*, 509.
[7] A. Ringk, X. Li, F. Gholamrezaie, E. C. P. Smits, A. Neuhold, A. Moser, C. Van der Marel, G. H. Gelinck, R. Resel, D. M. de Leeuw, P. Strohriegl, *Adv. Funct. Mater.* **2013**, *23*, 2016.
[8] P. Yang, R. Yan, M. Fardy, *Nano Lett.* **2010**, *10*, 1529.
[9] E. Stern, J. F. Klemic, D. A. Routenberg, P. N. Wyrembak, D. B. Turner-Evans, A. D. Hamilton, D. A. LaVan, T. M. Fahmy, M. A. Reed, *Nature* **2007**, *445*, 519.
[10] X. Duan, N. K. Rajan, M. H. Izadi, M. A. Reed, *Nanomed.* **2013**, *8*, 1839.
[11] J. Satija, V. V. R. Sai, S. Mukherji, *J. Mater. Chem.* **2011**, *21*, 14367.
[12] X. Duan, N. K. Rajan, D. A. Routenberg, J. Huskens, M. A. Reed, *ACS Nano* **2013**, *7*, 4014.
[13] M. M. Hakim, M. Lombardini, K. Sun, F. Giustiniano, P. L. Roach, D. E. Davies, P. H. Howarth, M. R. de Planque, H. Morgan, P. Ashburn, *Nano Lett.* **2012**, *12*, 1868.
[14] U. Jönsson, G. Olofsson, M. Malmqvist, I. Rönnberg, *Thin Solid Films* **1985**, *124*, 117.
[15] B. Arkles, J. Steinmetz, J. Zazyczny, P. Mehta, *J. Adhes. Sci. Technol.* **1992**, *6*, 193.
[16] E. L. Schmid, T. A. Keller, Z. Dienes, H. Vogel, *Anal. Chem.* **1997**, *69*, 1979.
[17] P. Jonkheijm, D. Weinrich, H. Schroder, C. M. Niemeyer, H. Waldmann, *Angew. Chem., Int. Ed. Engl.* **2008**, *47*, 9618.
[18] S. P. Pujari, L. Scheres, A. Marcelis, H. Zuilhof, *Angew. Chem. Int. Ed.* **2014**, *53*, 6322.
[19] M. Schena, D. Shalon, R. W. Davis, P. O. Brown, *Science* **1995**, *270*, 467.
[20] G. L. Kenausis, J. Vörös, D. L. Elbert, N. Huang, R. Hofer, L. Ruiz-Taylor, M. Textor, J. A. Hubbell, N. D. Spencer, *J. Phys. Chem. B* **2000**, *104*, 3298.
[21] J. Fritz, E. B. Cooper, S. Gaudet, P. K. Sorger, S. R. Manalis, *Proc. Natl. Acad. Sci. U.S.A.* **2002**, *99*, 14142.
[22] L. Ruiz-Taylor, T. Martin, F. Zaugg, K. Witte, P. Indermuhle, S. Nock, P. Wagner, *Proc. Natl. Acad. Sci. U.S.A.* **2001**, *98*, 852.
[23] S. Morgenthaler, C. Zink, B. Städler, J. Vörös, S. Lee, N. D. Spencer, S. G. Tosatti, *Biointerphases* **2006**, *1*, 156.
[24] S. Gon, M. M. Santore, *Langmuir* **2011**, *27*, 15083.
[25] E. Stern, R. Wagner, F. J. Sigworth, R. Breaker, T. M. Fahmy, M. A. Reed, *Nano Lett.* **2007**, *7*, 3405.
[26] K. L. Prime, G. M. Whitesides, *J. Am. Chem. Soc.* **1993**, *115*, 10714.
[27] M. Zheng, F. Davidson, X. Huang, *J. Am. Chem. Soc.* **2003**, *125*, 7790.
[28] H. U. Khan, J. Jang, J. J. Kim, W. Knoll, *Biosens. Bioelectron.* **2011**, *26*, 4217.
[29] L. S. Jung, K. E. Nelson, P. S. Stayton, C. T. Campbell, *Langmuir* **2000**, *16*, 9421.
[30] X. X. Duan, Y. Li, N. K. Rajan, D. A. Routenberg, Y. Modis, M. A. Reed, *Nat. Nanotechnol.* **2012**, *7*, 401.
[31] Y. C. Liu, N. Rieben, L. Iversen, B. S. Sorensen, J. Park, J. Nygard, K. L. Martinez, *Nanotechnology* **2010**, *21*, 245105.
[32] M. Zhu, M. Z. Lerum, W. Chen, *Langmuir* **2011**, *28*, 416.